Heterogeneity of Astrocyte and NG2 Cell Insertion at the Node of Ranvier

David R. Serwanski, Peter Jukkola, and Akiko Nishiyama*

Department of Physiology and Neurobiology, University of Connecticut, Storrs, Connecticut 06269

ABSTRACT

The node of Ranvier is a functionally important site on the myelinated axon where sodium channels are clustered and regeneration of action potentials occurs, allowing fast saltatory conduction of action potentials. Early ultrastructural studies have revealed the presence of "glia" or "astrocytes" at the nodes. NG2 cells, also known as oligodendrocyte precursor cells or polydendrocytes, which are a resident glial cell population in the mature mammalian central nervous system that is distinct from astrocytes, have also been shown to extend processes that contact the nodes. However, the prevalence of the two types of glia at the node has remained unknown. We have used specific cell surface markers to examine the association of NG2 cells and astrocytes with the nodes of Ranvier in the optic nerve, corpus callosum, and spinal cord of young adult mice or rats. We show that more than 95% of the nodes in all three regions contained astrocyte processes, while 33–49% of nodes contained NG2 cell processes. NG2 cell processes were associated more frequently with larger nodes. A few nodes were devoid of glial apposition. Electron microscopy and stimulated emission depletion (STED) super-resolution microscopy confirmed the presence of dual glial insertion at some nodes and further revealed that NG2 cell processes contacted the nodal membrane at discrete points, while astrocytes had broader processes that surrounded the nodes. The study provides the first systematic quantitative analysis of glial cell insertions at central nodes of Ranvier. J. Comp. Neurol. 000:000–000, 2016.

© 2016 Wiley Periodicals, Inc.

INDEXING TERMS: astrocyte; oligodendrocyte; node of Ranvier; glia; NG2; myelin; RRID: AB_10697718; RRID: AB_10671175; RRID: AB_2572297; RRID: AB_2057371; RRID: AB_10013382; RRID: AB_90959; RRID: AB_2571717; RRID: AB_2572299; RRID: AB_2572306; RRID: AB_91789; RRID: AB_477552

The myelinated axon is composed of regularly spaced myelinated internodes separated by the nodes of Ranvier, where sodium channels are clustered at a high density, allowing for fast saltatory conduction of action potentials. Axons of neocortical neurons are only partially myelinated in adults (Tomassy et al., 2014), and myelination continues throughout life. Newly formed internodes are shorter than existing internodes (Young and Richardson, 2013), and the average internode length decreases with age (Lasiene et al., 2009). These changes could have profound effects on the proper function of the neural circuit, as the efficiency of impulse conduction is a function of internode length (Brill et al., 1977; Seidl et al., 2010).

The node of Ranvier is formed and maintained by interactions among the axonal membrane, the underlying cytoskeleton, and the surrounding glial cell membranes and extracellular matrix (Normand and Rasband, 2015). In addition to the myelinating oligodendrocytes, two other macroglial cell types, astrocytes and NG2 cells, are intimately associated with myelinated axons. Astrocytes primarily function to clear neurotransmitters and K+ released during synaptic transmission (Kimelberg, 2010). NG2 cells, also known as oligodendrocyte precursor cells or polydendrocytes, are morphologically, antigenically, and functionally distinct from white matter astrocytes (Peters, 2004; Nishiyama et al., 2009; Hill and Nishiyama, 2014). They express voltage-dependent

© 2016 Wiley Periodicals, Inc.

Additional Supplementary Material may be found in the online version of this article.

The first two authors contributed equally to this work.

Grant sponsor: National Institutes of Health; Grant numbers: R01 NS73425; R01 NS049267 (both to A.N.); Grant sponsor: National Multiple Sclerosis Society; Grant numbers: A2826; RG4579 (both to A.N.).

*CORRESPONDENCE TO: Akiko Nishiyama, Department of Physiology and Neurobiology, University of Connecticut, 75 North Eagleville Road, Unit 3156, Storrs, CT 06269-3156. E-mail: akiko.nishiyama@uconn.edu

Received August 13, 2015; Revised July 12, 2016;
Accepted July 12, 2016.
DOI 10.1002/cne.24083
Published online Month 00, 2016 in Wiley Online Library (wileyonlinelibrary.com)

TABLE 1.
Primary Antibodies Used in This Study

Antibody	Immunogen	Manufacturer, RRID, Host, and clonality	Dilution
AnkG	Full-length human ankyrin G (~1,000 amino acids)	UC Davis/NIH NeuroMab Facility (Davis, CA), Cat# 73-146, RRID: AB_10697718 Mouse monoclonal antibody (clone N106/36)	1:50
Caspr	QNHRYKGSYHTNEPKATHDSH PGGKAPLPPSGPAQAPAPTPAP TQVPTPAPAPASGPGPRDQNLPQILEESRS	UC Davis/NIH NeuroMab Facility Cat# 73-001 RRID: AB_10671175 Mouse monoclonal antibody (clone K65/35)	1:50
Caspr	Cytoplasmic domain of rat p190/ contactin-associated protein	Dr. Matthew Rasband (Baylor College of Medicine, Houston, TX) RRID: AB_2572297 Rabbit polyclonal antibody	1:3,000
CC1	Amino acids 1–226 of human APC (Ab-7) (CC-1)	Calbiochem (Millipore, Billerica, MA), Cat#OP80 RRID: AB_2057371 Mouse monoclonal antibody (clone CC1)	1:100
GFAP	Bovine glial fibrillary acidic protein	Dako (Carpinteria, CA), Cat# Z0334 RRID: AB_10013382 Rabbit polyclonal antibody	1:2,000
GLAST	QLIAQDNEPEKPVADSETKM (C-terminus of glutamate–aspartate transporter)	Millipore, Cat# AB1782 RRID: AB_90959 Guinea pig polyclonal antibody	1:1,000
GLAST	KNRDVEMGNSVIEENEMKKPYQLIA QDNEPEKPVADSETKMmouse GLAST, C-terminal 41 amino acids	Frontier Institute (Ishikari, Hokkaido, Japan), Cat# GLAST-GP RRID: AB_2571717 Guinea pig polyclonal antibody	1:1,000
NG2	Extracellular domain of rat NG2, amino acids 30–2,225	Dr. William Stallcup (Sanford Burnham Prebys Medical Discovery Institute, La Jolla, CA) RRID: AB_2572299 Guinea pig polyclonal antibody	1:1,000
NG2	Extracellular domain of rat NG2, amino acids 30–2,225	Dr. William Stallcup RRID: AB_2572306 Rabbit polyclonal antibody	1:1,000
NG2	Purified rat NG2 chondroitin sulfate proteoglycan	Millipore, Cat# AB5320 RRID: AB_91789 Rabbit polyclonal antibody	1:500
Pan-NaCh	CTEEQKKYYNAMKKLGSKK (intracellular loop III–IV of sodium channel α subunit)	Sigma-Aldrich (St. Louis, MO), Cat# S8809 RRID: AB_477552 Mouse monoclonal antibody (clone K58/35)	1:100

ion channels and neurotransmitter receptors and respond to vesicularly released neurotransmitter (Bergles et al., 2010), but their role in the neural network is unknown.

Glial processes have been seen at the node of Ranvier in a variety of species (Hildebrand, 1971; Waxman and Swadlow, 1976; Waxman and Black, 1984), and the astrocyte-specific glial filaments were detected in some of the nodal glia (ffrench-Constant et al., 1986). More recent work by Butt and colleagues (1999) demonstrated that processes of NG2 cells also contact the node of Ranvier. However, the frequency at which the processes from NG2 cells and astrocytes exist at the node has remained unclear. Here we show by confocal microscopy that nearly all of the nodes in the adult optic nerve, corpus callosum, and spinal cord contain processes from astrocytes, while fewer than one-half of nodes are contacted by both NG2 cell and astrocyte processes. Ultrastructural analysis revealed that NG2 cells extend fine finger-like projections that often contact both the nodal axolemma and outermost paranodal myelin loops, while astrocytes extend broader processes covering the entire nodal gap, suggesting different roles of the two glial cell types at the node.

MATERIALS AND METHODS

Antibody characterization

See Table 1 for further details.

Mouse anti-ankyrin G (AnkG) monoclonal antibody was obtained from the UC Davis/NIH NeuroMab Facility. It was generated using a fusion protein containing ~1,000 amino acids of the full-length human Ankyrin G sequence (Damiani et al., 2012; AN King et al., 2014). This cell culture supernatant antibody recognizes a single large band at 250 kDa on western blot (Brandao

et al., 2012), and yields a characteristic staining pattern for the axon initial segment and the nodes of Ranvier in our studies and in those of others (Gasser et al., 2012; Amor et al., 2014).

Mouse anti–contactin-associated protein (Caspr) monoclonal antibody was obtained from the UC Davis/NIH NeuroMab Facility and was used in Figures 4–7. This supernatant antibody was generated from the cytoplasmic domain (amino acids 1,308–1,381) of rat Caspr protein, and yields a single band of ~220 kDa on western blots of mouse brain homogenates (Dagley et al., 2014). The antibody yields a characteristic paranodal staining pattern in myelinated tissues in our studies, as previously reported by others (Gasser et al., 2012).

Rabbit anti-Caspr antibody was a gift from Dr. Matthew Rasband (Baylor College of Medicine) and was used in Figures 2 and 3. This affinity-purified antibody was generated against a fusion protein containing the entire cytoplasmic domain of rat p190/Caspr protein (Peles et al., 1997; Schafer et al., 2004), and recognizes a band at 190 kDa on western blot from brain tissues (Peles et al., 1997). Immunostaining with this antibody yielded the characteristic paranodal staining pattern and distribution in myelinated tissues in our studies and in those of others, similar to the mouse anti-Caspr antibody (Rasband et al., 1999, 2003; Schafer et al., 2004).

Mouse monoclonal anti-APC antibody (clone CC1) was obtained from Calbiochem (Millipore, Billerica, MA). It was generated against amino acids 1–226 of recombinant human APC and recognizes a single band of 300 kDa by western blot (Bhat et al., 1996). Current and previous immunostaining studies in our laboratory have revealed cells with characteristic oligodendrocyte morphology and distribution (Zhu et al., 2008; Komitova et al., 2009, 2011).

Rabbit anti-glial fibrillary acidic protein (GFAP) polyclonal antibody was obtained from Dako (Carpinteria, CA). It was generated against purified GFAP from bovine spinal cord and recognizes a ~50-kDa band in rat dorsal root ganglion homogenates (Yamanaka et al., 2011). Immunohistochemical studies using this antibody in mouse brain tissue revealed cells with characteristic astrocyte morphology and distribution (Komitova et al., 2011).

Guinea pig anti-glutamate–aspartate transporter (GLAST) polyclonal antibody was obtained from Chemicon (Millipore) and was used in Figures 1–3. This antibody was generated with a synthetic peptide of 19 amino acids from the C-terminus of rat GLAST, and recognized a 65-kDa band on a western blot of rat brain tissue (Chung et al., 2008). Immunohistochemical studies in rat striatum (Chung et al., 2008) and cerebellum (Douyard et al., 2007) tissues revealed staining characteristic of gray matter astrocytes in addition to the white matter fibrous astrocyte population labeled in our studies.

A second guinea pig anti-GLAST polyclonal antibody was obtained from the Frontier Institute (Ishikari, Hokkaido, Japan) and was used in Figures 4–7. This affinity-purified antibody was generated against the C-terminal 41 amino acids of mouse GLAST protein and recognizes a 60-65-kDa band on western blots from adult mouse brain membrane extracts (Shibata et al., 1997). Immunostaining using this antibody reveals developing and mature astrocytes in mouse spinal cord (Shibata et al., 1997) and other tissues, and the astrocyte morphology and distribution patterns observed in our studies agreed with those observed using the guinea-pig anti-GLAST antibody from Millipore.

Rabbit anti-NG2 polyclonal antibody was a gift from Dr. William Stallcup (Sanford Burnham Prebys Medical Discovery Institute),and was used in Figures 1 and 8. This antibody was generated using a recombinant protein comprising the full extracellular domain of rat NG2, amino acids 30–2,225, and recognized a ~260-kDa band in a western blot of lysates from GD25 cells transfected with NG2 cDNA (Tillet et al., 2003). In current and previous studies in our lab, immunolabeling with this antibody resulted in characteristic NG2 cell morphology and distribution patterns in mouse and rat CNS tissue (Zhu et al., 2008; Komitova et al., 2009).

Guinea pig anti-NG2 polyclonal antibody was also a gift from Dr. William Stallcup, and was used in Figure 2. This antibody was raised against the same extracellular domain of rat NG2 as described above for the rabbit anti-NG2 antibody and resulted in the same staining pattern in our current and previous studies on rat and mouse central nervous system (CNS) tissue (Zhu et al., 2008; Komitova et al., 2009).

Rabbit anti-NG2 chondroitin sulfate proteoglycan antibody was obtained from Millipore and was used in Figures 4–7. This antibody was generated using purified rat NG2 chondroitin sulfate proteoglycan, and it recognizes both the intact proteoglycan and the 300-kDa NG2 core glycoprotein (Komitova et al., 2009). Immunostaining with this antibody yielded a labeling pattern and distribution characteristic of NG2 cells in this and previous studies, in agreement with the results obtained using the rabbit and guinea-pig anti-NG2 ectodomain antibodies received from Dr. Stallcup (Komitova et al., 2009, 2011).

Mouse anti-pan-sodium channel (NaCh) monoclonal antibody was obtained from Sigma-Aldrich (St. Louis, MO). It was generated using a 19-amino acid peptide

from the sodium channel intracellular loop III–IV (C. King et al., 2014). It recognizes a 260-kDa band in western blots of rat brain extracts, corresponding to the size of the sodium channel α subunit (CH King et al., 2014). Immunolabeling with this antibody reveals the axon initial segment and the nodes of Ranvier throughout the mouse and rat central and peripheral nervous systems (Rasband et al., 1999; Amor et al., 2014; CH King et al., 2014).

Immunofluorescence labeling

Postnatal day 30 (P30) Sprague–Dawley rats and P30 C57Bl/6 mice were anesthetized with isoflurane and perfused with a fixative consisting of 2% or 4% paraformaldehyde, 0.1 M lysine, and 0.02 M sodium metaperiodate (PLP fix; McLean and Nakane, 1974). The brains, optic nerves, and spinal cords were dissected and postfixed in the same fixative for 1 hour at 4°C. Tissues were then rinsed in 0.2 M sodium phosphate buffer, pH 7.2, cryoprotected in 30% sucrose, and embedded in OCT compound (optimum cutting temperature, Tissue-Tek, Sakura Finetek, Torrance, CA). Longitudinal 10- or 20-μm sections of the optic nerve and coronal sections through the anterior corpus callosum were cut on a cryostat (Microm HM500 or Leica CM 3050 S).

For light microscopy, sections were rinsed in phosphate-buffered saline (PBS) and then blocked and permeabilized in PBS containing 5% normal goat serum (NGS) or 0.3% bovine serum albumin (BSA) and 0.1% Triton X-100 for 1 hour at RT. The sections were then incubated in primary antibodies overnight at 4°C. After three rinses in PBS, the sections were incubated in secondary antibodies. Secondary antibodies for triple labeling were: Cy3-labeled donkey anti-guinea pig or rabbit (1:200; Jackson ImmunoResearch, West Grove, PA), Cy5-labeled donkey anti-rabbit (1:50; Jackson ImmunoResearch), and Alexa 488-conjugated goat anti-mouse IgG (1:1,000; Molecular Probes, Eugene, OR). Secondary antibodies for quadruple labeling (all from Invitrogen, Carlsbad, CA) were Alexa 488-conjugated goat anti-mouse IgG subclass 2a (for AnkG), Alexa 532-conjugated goat anti-rabbit (for NG2), Alexa 594-conjugated goat anti-guinea pig (for GLAST), and Alexa 647-conjugated goat anti-mouse IgG subclass 1 (for Caspr). Labeled sections were mounted in Vectashield (Vector, Burlingame, CA) and examined using a Leica TCS SP2 or TCS SP8 confocal microscope, or a Zeiss Axiovision 200M equipped with the ApoTome grid confocal system and the ORCA ER camera (Hamamatsu, Bridgewater, NJ). Three-dimensional (3D) volume renderings were produced using Leica Application Suite (LAS AF version 4.0) software, from *z*-stack images of P30 mouse optic nerve or spinal cord collected at 0.3- or 0.5-μm intervals on a Leica TCS SP8 confocal microscope system.

STED super-resolution imaging

Super-resolution images were collected on a demo Leica SP8 stimulated emission depletion (STED) 3X microscope system with tunable white light laser, a 100× objective, and two depletion laser beams. Sections were stained as described above for quadruple labeling and were mounted in Prolong Diamond (Invitrogen). STED images were obtained for GLAST and Caspr using the 770-nm pulsed depletion laser beam and for NG2 using the 660-nm gated depletion beam.

Pre-embedding immunoelectron microscopy

Anesthetized P30 Sprague–Dawley rats or P30 NG2DsRedBAC transgenic mice were perfused at room temperature with 10 ml Ringer's solution, pH 7.0, followed by 100 ml of the fixative containing 4% paraformaldehyde and 0.1% glutaraldehyde in 0.1 M phosphate buffer (PB), pH 7.4. The optic nerves and brains were dissected and postfixed for 1 hour at 4°C using the same fixative. They were then washed in PB, and 50-μm longitudinal sections of optic nerves and coronal sections of corpus callosum were cut in ice-cold PBS using a Leica VT1000 Vibroslicer. The sections were then put into nylon meshed buckets inserted into 12-well tissue culture plates and blocked for 1 hour at room temperature using 3% NGS/PBS blocking solution. Sections were then incubated overnight at 4°C in rabbit antibody to NG2 or guinea pig antibody to GLAST, each diluted 1:1,000 in PBS/NGS. Tissue sections that were not incubated in primary antibody were used as negative controls. The ABC/peroxidase reaction was used to detect the primary antibody where diaminobenzidine (DAB) was used as the chromogen (Vectastain Elite kit, Vector). Sections were washed in PBS and incubated in 1% OsO_4/0.1 M cacodylate buffer for 30 minutes at room temperature. After a thorough rinsing in dH_2O, the sections were dehydrated and infiltrated in Embed-812 resin (EM Sciences, Hatfield, PA). Sections were then flat-embedded between two sheets of Aclar film and polymerized at 60°C for 48 hours.

Thin sections of 70-nm thickness were cut on a Leica Ultracut microtome and placed on 200-mesh copper grids. The sections were counterstained with 2% aqueous uranyl acetate and Sato's lead citrate for 5 and 3 minutes, respectively. The sections were viewed using a FEI Technai Biotwin electron microscope at 80 kV and images were acquired digitally.

Quantification

The percentage of the nodes that were contacted by an NG2+ or a GLAST+ process was obtained from sections quadruple labeled for NG2, GLAST, Caspr, and

AnkG. Stacks of *z*-slices were collected from the middle segment of the optic nerves (rat), the thoracic ventral spinal cord white matter (mouse), or the midline region of the anterior corpus callosum at the level of the anterior commissure (mouse) on a Leica SP8 TCS confocal imaging system. We used a 100× objective to collect a series of 0.3-µm-confocal *z*-stacks spanning 6–10 µm from random fields in each anatomical region and scored each node in the volume for the presence of glial processes. A node was identified by an AnkG cluster flanked on both sides by Caspr immunoreactivity. With the NG2 and the GLAST channels hidden to eliminate bias, 15–30 nodes per field of view were chosen and marked for further analysis. To ensure that the entire node was present in the *z*-stacks, nodes were analyzed only if more than one *z*-section existed below and above the AnkG/Caspr-stained node/paranodal structure. With the NG2 channel hidden, each node was scored as either containing or not containing a GLAST+ process. Then, with the GLAST channel hidden, the same nodes were scored as either containing or not containing an NG2+ glial process. Values are expressed as averages ± standard error of the mean (SEM).

RESULTS

Light microscopic analysis of nodal contact by glial cell processes

Glial cells in the optic nerve

Longitudinal sections of optic nerves from P30 rats were immunolabeled for NG2 or GLAST to examine the distribution of the two glial cells in the nerve. NG2 labeling showed a uniform distribution of labeled cells throughout the entire length of the nerve. The labeled cells displayed the typical polydendrocyte morphology with elongated cell bodies and multiple delicate processes oriented both longitudinally and transversely (Fig. 1A). Some of these cells were located within rows of oligodendrocytes, identified by the monoclonal antibody CC1 (Bhat et al., 1996), while others were located between the oligodendrocyte rows. Most of the NG2 cells had elongated cell bodies oriented parallel to the axons. Many of their processes extended longitudinally while others were oriented more radially.

NG2 cells comprised a distinct glial population from astrocytes that were labeled with anti-GLAST antibody (Fig. 1B). GLAST+ astrocytes were distributed uniformly throughout the nerve, and their processes were thicker than those of NG2+ processes. They extended in both longitudinal and transverse orientations, and their transverse processes were more prominent than those of NG2 cells. Double labeling of sections with guinea pig anti-GLAST and rabbit anti-GFAP antibodies showed a high degree of overlap between the two labels, indicating that GLAST could be used as a reliable cell surface marker for astrocytes (Fig. 1C).

Both NG2 cells and astrocytes contact nodes of Ranvier

To determine the prevalence of NG2 cells and astrocytes at the nodes of Ranvier, we labeled sections from P30 rat optic nerves for sodium channel, Caspr, and either NG2 or GLAST. A node was identified as a sodium channel cluster flanked on both sides by Caspr immunoreactivity. At some nodes, both sodium channel and Caspr immunoreactivity could be seen as double lines parallel to the orientation of the axons (Figs.

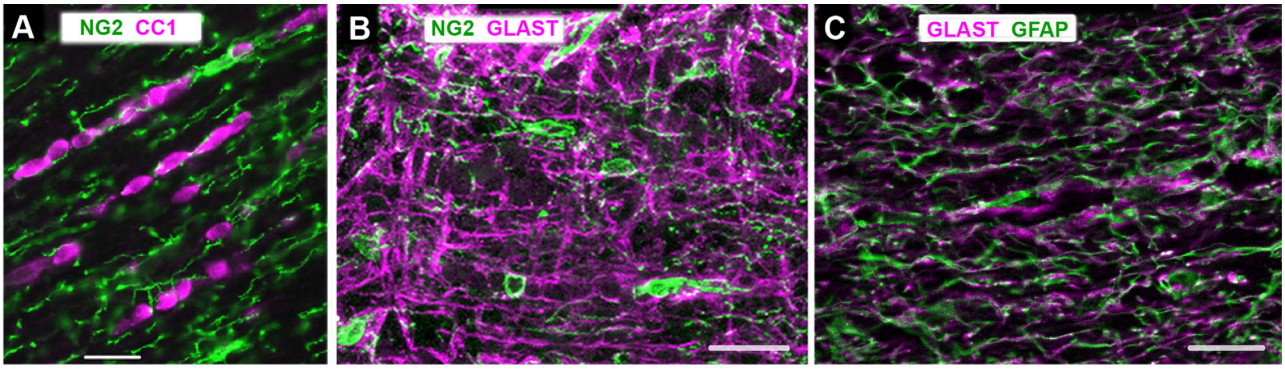

Figure 1. Glial cells in longitudinal sections of P30 rat optic nerves. **A:** Cells double-labeled with rabbit anti-rat NG2 (green) and mouse CC1 antibody (magenta) that recognizes oligodendrocytes. **B:** Cells double-labeled with rabbit anti-rat NG2 (green) and guinea pig anti-GLAST (magenta) antibodies. NG2 cells and GLAST+ astrocytes represent non-overlapping cell populations. **C:** Cells double-labeled with rabbit anti-GFAP (green) and guinea pig anti-GLAST antibodies (magenta). GLAST and GFAP immunoreactivity are colocalized. A: acquired by wide-field microscopy. B and C: stacks of confocal images. Scale bar = 20 µm in A–C.

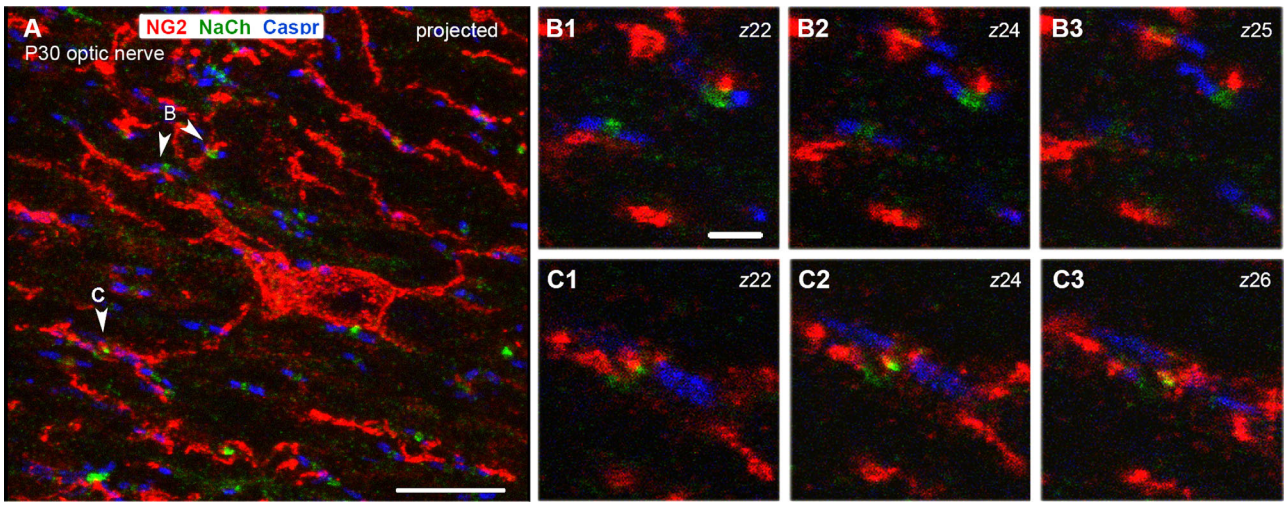

Figure 2. P30 rat optic nerve section triple labeled for NG2, sodium channel (NaCh), and Caspr. **A:** A projected image showing an NG2-labeled cell in the center (red) extending processes in longitudinal and transverse orientations. Numerous nodes of Ranvier detected by a Na+ channel cluster (green) flanked by Caspr+ paranodes (blue) are scattered throughout the field. **B1–B3:** Single *z*-slices through the nodes shown by arrowheads marked B in A. **C1–C3:** Single *z*-slices through the node shown by arrowhead marked C in A. NG2+ processes are closely associated with the node in C and the upper node in B. The numbers in the upper right indicate the positions of the *z*-slice. Scale bar = 10 μm in A; 2 μm in B1 (applies to B1–C3).

2 and 3). NG2 cells were distributed throughout the optic nerve, radially extending thin processes that frequently ran parallel with the axons. In many places, these processes were closely associated with nodal sodium channel immunolabeling (Fig. 2). When GLAST antibody was used with antibodies to sodium channel and Caspr, GLAST+ astrocytes were also found to be distributed throughout the optic nerve, with longer and thicker processes running along axons and closely associated with sodium channel immunolabeling at the nodes of Ranvier (Fig. 3). We also observed a similar association of NG2 cell and GLAST+ astrocyte processes with the nodes of Ranvier in P30 rat corpus callosum (not shown).

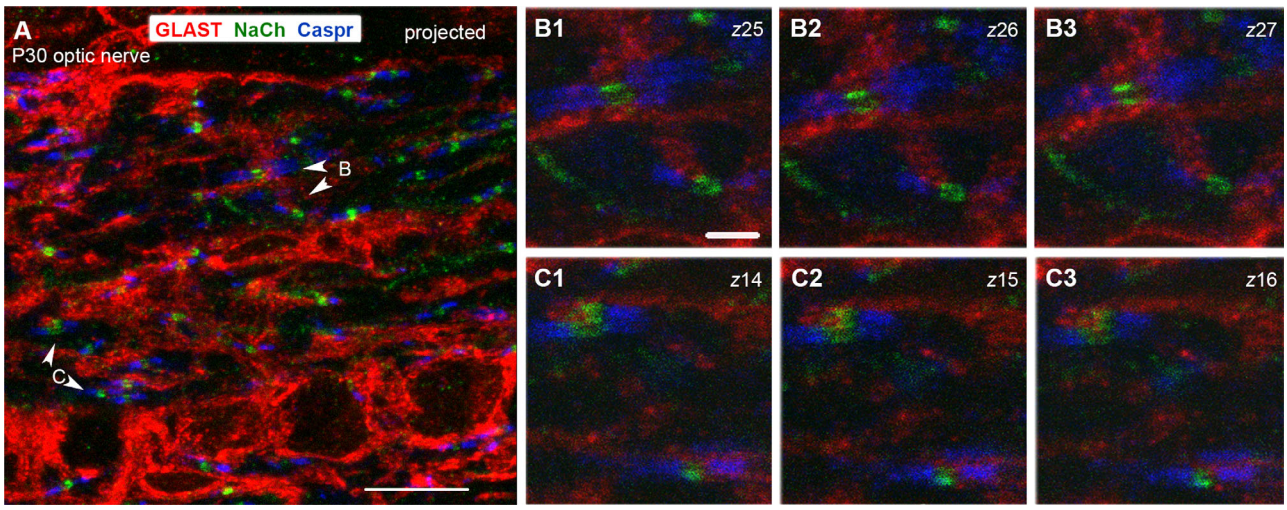

Figure 3. P30 rat optic nerve section triple labeled for GLAST, sodium channel (NaCh), and Caspr. **A:** A projected image showing several GLAST-labeled (red) cell bodies in the bottom and thick GLAST+ processes in longitudinal and transverse orientations. Numerous nodes of Ranvier detected by an Na+ channel cluster (green) flanked by Caspr+ paranodes (blue) are scattered throughout the field. **B1-B3:** Single *z*-slices through the nodes shown by arrowheads marked B in A. **C1–C3**: Single *z*-slices through the node shown by arrowheads marked C in A. GLAST+ processes are closely associated with all the nodes in B and C. The numbers in the upper right indicate the positions of the *z*-slice. Scale bar = 10 μm in A; 2 μm in B1 (applies to B1–C3).

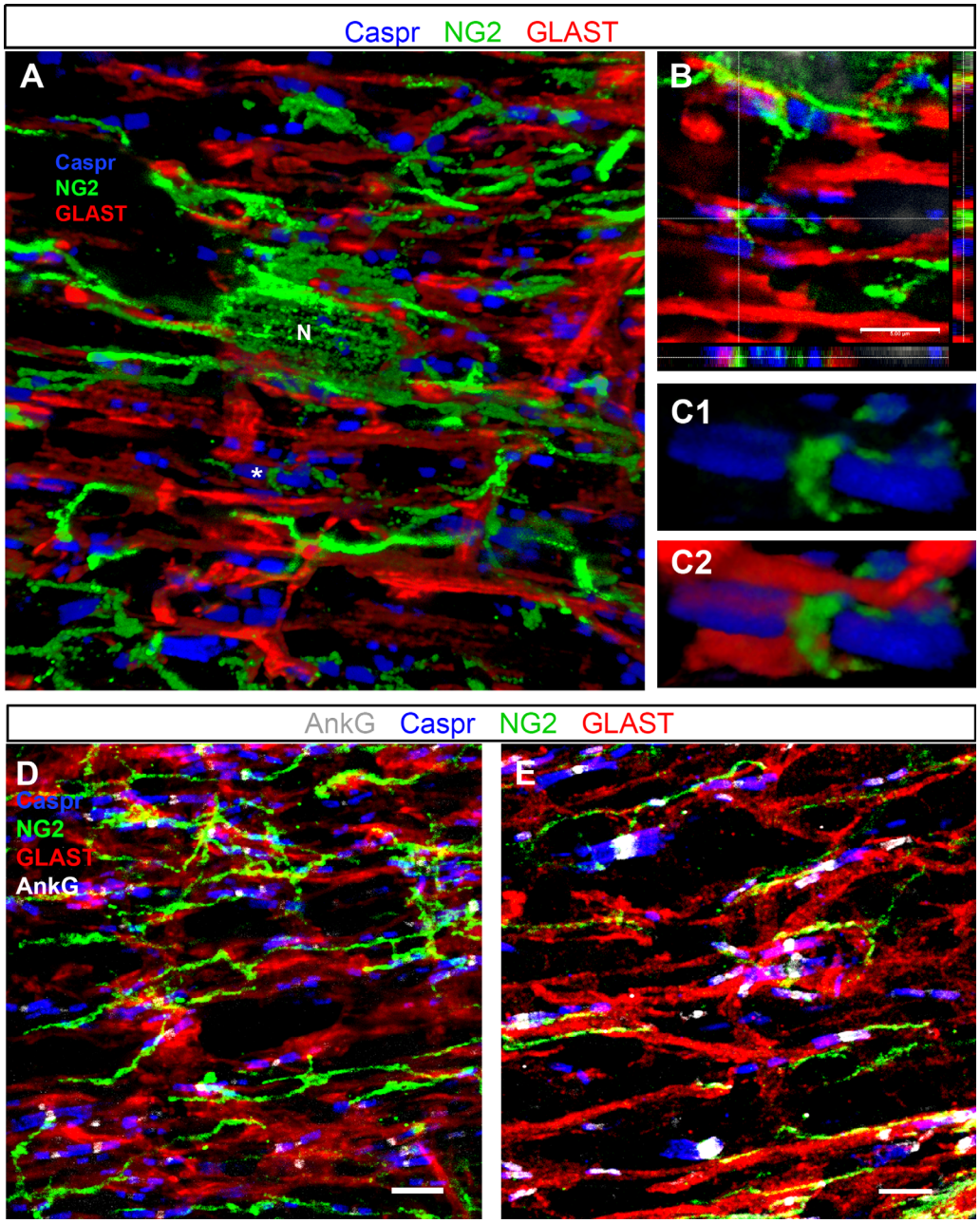

Figure 4. Triple and quadruple immunostaining of P30 optic nerve and thoracic spinal cord. **A–C:** P30 mouse optic nerve section triple labeled with anti-NG2 (green), GLAST (red), and Caspr (blue) antibodies. **A:** A 3D volume rendering showing many Caspr+ paranodal pairs in contact with or flanking glial processes labeled with antibodies to NG2 and GLAST. Several processes from the same NG2 cell (N) are shown to contact different nodes of Ranvier. **B:** Single *z*-plane images in three dimensions show NG2+ and GLAST+ processes positioned directly between Caspr+ paranodes, presumably in close contact with the node (shown with * in A). Image taken from the same *z*-stack as the volume rendering in A. **C1,C2:** A 3D volume rendering of the node shown at the crosshairs in B, showing clear insertion of the NG2+ process between the Caspr+ paranodes (C1). The same node is shown in C2 along with the GLAST+ astrocyte processes. **D,E:** Quadruple immunostaining of P30 rat optic nerve (D) and P30 mouse thoracic spinal cord white matter (E) sections labeled with AnkG (white), NG2 (green), GLAST (red), and Caspr (blue) antibodies. Images are confocal maximum projections of *z*-stack images. GLAST+ (astrocyte) and NG2+ cell processes contact the AnkG+ nodes, flanked by Caspr+ paranodes. Scale bar = 5 μm in A, B, D, E; 1 micrometer in C.

To determine whether NG2+ and GLAST+ processes contacted the same nodes, we initially performed confocal microscopy with 3D volume rendering on 20-μm sections from P30 mouse optic nerves that were triple labeled for NG2, GLAST, and Caspr (Fig. 4A–C). A subpopulation of the nodes, identified as gaps in Caspr

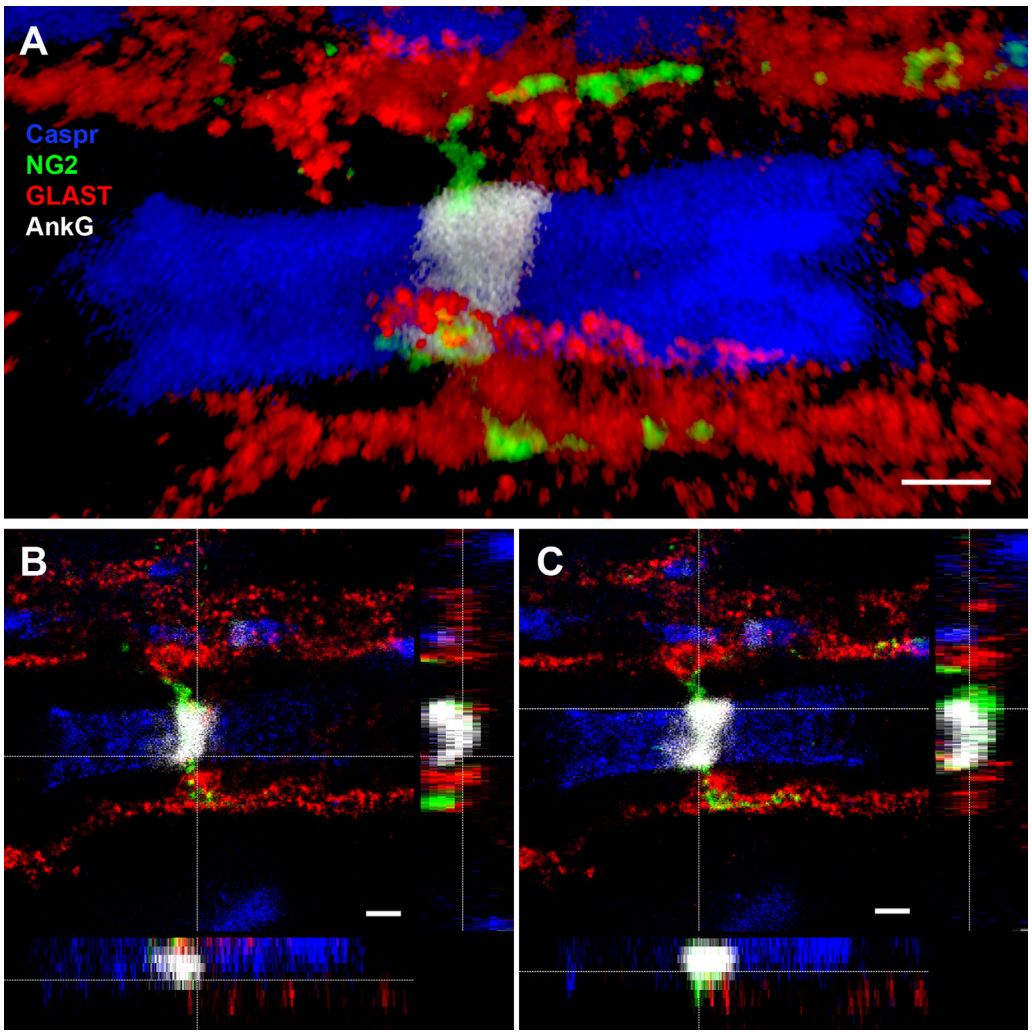

Figure 5. Super-resolution image of node of Ranvier in the mouse thoracic spinal cord. STED confocal images showing the close association of both astrocyte (GLAST, red) and NG2 cell (NG2, green) processes with the node (AnkG, white), flanked by paranodes (Caspr, blue). **A:** 3D volume rendering of glial contact at the node. **B:** Orthogonal views of the node, showing astrocyte (GLAST, red) contact at the node (AnkG, white). **C:** Orthogonal views of the node, showing NG2 cell (NG2, green) contact at the node (AnkG, white). The NG2 cell process appeared to wrap closely around the node of Ranvier. Scale bar = 1 μm in A–C.

staining, appeared to have both NG2 cell and astrocyte processes associated with them. In such nodes, astrocytes typically appeared as broad sheet-like processes that wrapped the nodes. By contrast, NG2 cell processes appeared at the nodal membrane as thin projections. Some NG2 cell processes appeared to loop around one side of a node adjacent to the terminal paranodal loop (Fig. 4C; also see ultrastructural analysis in Fig. 9C).

Quadruple labeling and super-resolution microscopy to visualize NG2 cell and astrocyte processes at the node

To better assess the frequency of NG2 cell and astrocyte processes at the nodes of Ranvier, we performed quadruple labeling for NG2, GLAST, Caspr, and the nodal protein AnkG. This strategy provided robust staining for all four labels, suitable for confocal and 3D analysis and quantification of glial contact at the nodes. In P30 rat optic nerve, we observed a fairly uniform population of nodes of Ranvier regularly distributed throughout the nerve. NG2+ and GLAST+ glial processes were interspersed among and appeared to be associated with the nodes (Fig. 4D). In the mouse spinal cord white matter, the nodes were more variable in size, and NG2+ and GLAST+ processes appeared to be closely associated with them (Fig. 4E; Supplementary movie 1). In the corpus callosum, the nodes were uniformly small and regularly distributed, but some of them also received contact from NG2+ and GLAST+ processes (data not shown).

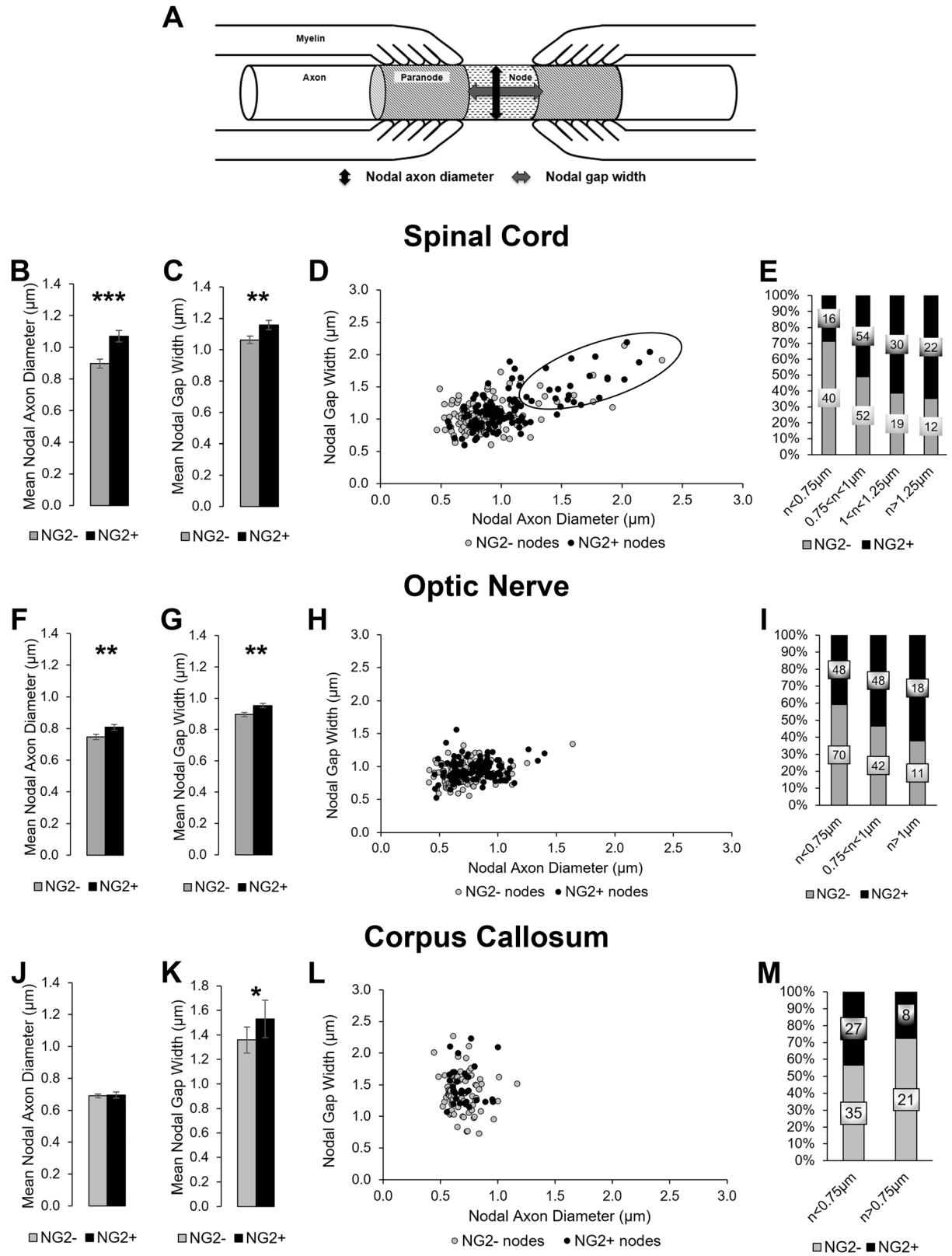

Figure 6. Quantification of NG2 cell processes at the node of Ranvier in different CNS regions. **A:** The cartoon illustrates the location of the node and paranodes along the axon in relation to the myelin membranes tethered to the axonal membrane. The two-way arrows show the measured distances for the nodal axon diameter (nAD) and the nodal gap width (nGW). **B–E:** NG2 cell contact in the thoracic spinal cord. **F–I:** NG2 cell contact in the optic nerve. **J–M:** NG2 cell contact in the corpus callosum. **B,F,J:** The mean nAD of nodes with or without NG2 cell processes. **C,G,K:** The mean nGW of nodes with or without NG2 cell processes. Mean ± SEM; ***, $P < 0.001$; **, $P < 0.01$; *, $P < 0.05$. **D,H,L:** Scatter plot showing nAD and nGW of each node of Ranvier with or without NG2 cell process. **E,I,M:** Stacked bar graph showing the percentage of nodes with or without NG2 cell processes separated into bins by nAD. The label on each bar indicates the number of scored nodes in each category.

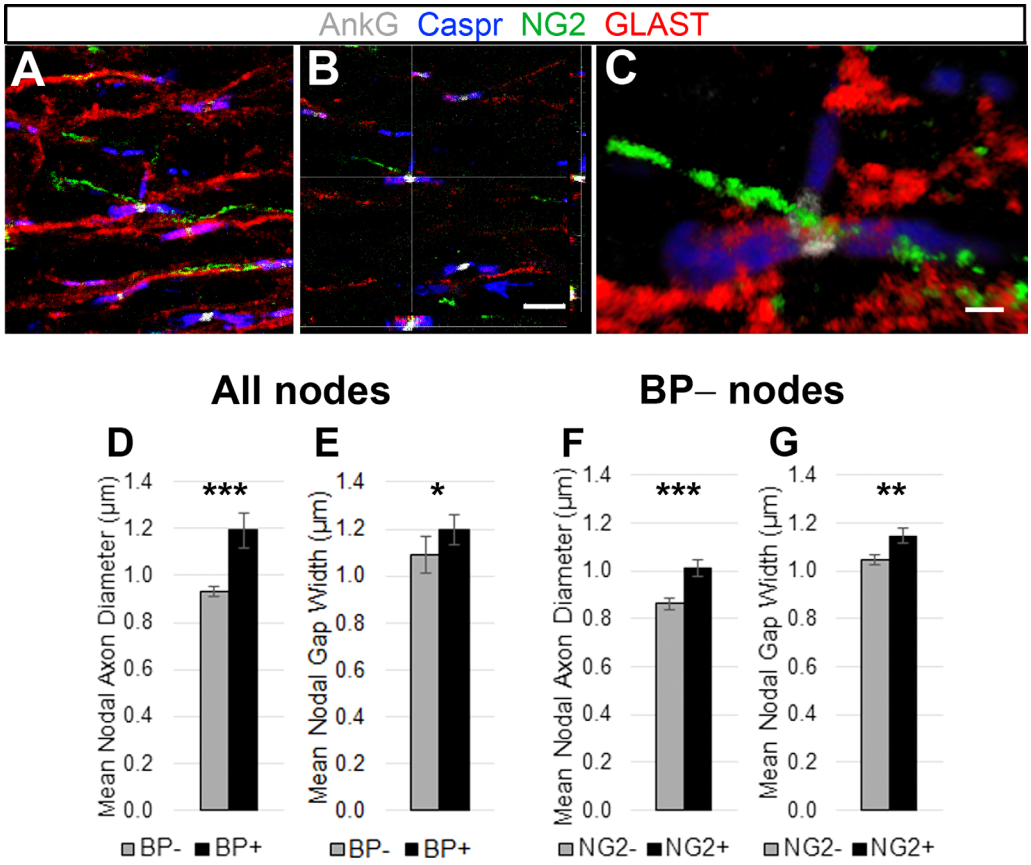

Figure 7. Quantification of nodes of Ranvier with axonal branchpoints in mouse thoracic ventral spinal cord white matter. **A–C:** Quadruple immunostaining of P30 mouse spinal cord white matter sections labeled with AnkG (white), NG2 (green), GLAST (red), and Caspr (blue) antibodies. GLAST+ (astrocyte) and NG2+ cell processes contact the AnkG+ nodes, flanked by Caspr+ paranodes. **A:** Confocal maximum projection of *z*-stack images, with an arrow indicating a node with a branchpoint leading to a third Caspr+ paranode. **B:** Orthogonal views of the branchpoint node indicated in A, showing astrocyte (GLAST, red) and NG2 cell (NG2, green) contact at the node (AnkG, white). **C:** 3D volume rendering of the branchpoint node indicated in A. **D,E:** Differences in the mean nAD (D) and nGW (E) of all the nodes with or without an axonal branchpoint. **F,G:** The mean nAD (F) and nGW (G) of nodes without branchpoints that had or did not have an NG2 cell process. Mean ± SEM; ***, $P < 0.001$; **, $P < 0.01$; *, $P < 0.05$. Scale bar = 5 µm in A,B; 1 µm in C.

To further assess the spatial relationship between astrocyte and NG2 cell processes and the node of Ranvier, we performed STED super-resolution confocal microscopy on longitudinal sections through the ventral funiculus of the mouse spinal cord using a Leica SP8 STED 3X microscope. The technique improved localization of the point source of the NG2 and GLAST fluorescent signals seen as a punctate pattern along the astrocyte or NG2 glial processes. STED confocal *z*-stacks were collected and visualized by 3D volume rendering (Fig. 5A) or by orthogonal views centered on nodes of Ranvier (Fig. 5B,C; see also Supplementary movie 2). This revealed close association of the GLAST+ and NG2+ processes with the node, likely to represent points of direct contact. The NG2 cell process in Figure 5 wrapped around a portion of the node, as shown by the orthogonal views of individual *z*-sections.

Quantification of glial cell association with the node of Ranvier

Astrocytes contact the majority of the nodes while NG2 cells contact 30–50% of the nodes

We next determined the prevalence of astrocyte and NG2 cell processes at the nodes of Ranvier. Quadruple immunolabeling for AnkG, Caspr, NG2, and GLAST was applied to longitudinal sections of the optic nerve, ventral funiculus of the spinal cord, and the midline region of the corpus callosum. Random fields were scanned using a 100× objective, and *z*-stacks were collected at 0.3-µm intervals through 6–10 µm of tissue. A node was identified as an AnkG+ cluster flanked on both sides by Caspr+ bands. These nodal structures were distributed evenly throughout the volume. As described in Materials and Methods, each node in the volume was scored for the presence or absence of astrocytes

and NG2 cell processes. In all three regions quantified, >95% of the scored nodes contained a GLAST+ astrocyte process, while 33–49% of nodes contained an NG2+ glial process (Table 2). Most of the nodes containing NG2+ processes also contained a GLAST+ process. Only a few nodes appeared to have neither astrocyte nor NG2 glial insertion, or to have NG2 glial insertion alone (data not shown).

NG2 cells prefer to contact larger nodes of Ranvier

We observed that only half of the nodes contained NG2 cell processes, possibly because NG2 cell processes contacted the nodes of local axons randomly, or because they specifically targeted nodes of certain physical properties. We determined whether there was a correlation between NG2 cell contact and the size of the nodes. The "nodal gap" refers to the space between the paranodes, where the terminal loops of the internodal myelin membranes are tethered to the axonal membrane. The axonal diameter and width of the nodal gap are important parameters that can influence the conduction velocity of myelinated axons. To obtain nodal axon diameter (nAD), we measured the length of a line drawn through an AnkG+ node perpendicular to the axons (Fig. 6A). To obtain nodal gap width (nGW), we measured the length of the AnkG+ node between the two paranode–node junctions on a line drawn parallel to the axon (Fig. 6A). These measurements were taken for each of the nodes marked and scored for glial contact.

In the spinal cord, we found that larger nodes were contacted by NG2+ processes more frequently. The mean nAD was greater in nodes with NG2 cell processes than those without (1.07 ± 0.04 μm, $n = 122$ vs. 0.90 ± 0.03 μm, $n = 123$ in nodes with and without NG2 cell processes, respectively), and the difference was statistically significant ($P < 0.001$; Fig. 6B). Similarly, the mean nGW was greater in nodes with NG2 cell processes than those without (1.16 ± 0.03, $n = 122$, vs. 1.06 ± 0.02 μm, $n = 123$ in nodes with and without NG2 cell processes, respectively), and the difference was statistically significant ($P < 0.01$; Fig. 6C). A scatterplot of the nAD and nGW of each scored node showed that the majority of the largest nodes contained NG2 cell processes (Fig. 6D). When the data were placed into bins based on nAD, the percentage of nodes receiving NG2 cell contact progressively increased from smallest to largest (Fig. 6E; 29% in nodes with nAD < 0.75 μm, 51% in nodes with nAD between 0.75 and 1.0 μm, 61% in nodes with nAD between 1.0 and 1.25 μm, and 65% in nodes with nAD > 1.25 μm).

In the optic nerve, despite a smaller average axonal size, larger nodes were contacted by NG2+ processes more frequently, although the correlation was less pronounced than that in the spinal cord. The mean nAD was significantly greater in nodes with NG2 cell processes than those without (Fig. 6F; 0.81 ± 0.02 μm, $n = 114$ vs. 0.74 ± 0.02 μm, $n = 123$ in nodes with and without NG2 cell processes, respectively, $P < 0.01$). Similarly, the mean nGW was greater in nodes with NG2 cell processes than those without (Fig. 6G; 0.95 ± 0.01, $n = 114$, vs. 0.90 ± 0.01 μm, $n = 123$ in nodes with and without NG2 cell processes, respectively, $P < 0.01$). A scatterplot of the nAD and nGW also revealed a slight tendency for the larger nodes to have NG2+ processes (Fig. 6H). When the data were placed into bins based on nAD, the percentage of nodes receiving NG2 cell contact progressively increased from smallest to largest (Fig. 6I; 41% of nodes with nAD < 0.75 μm, 53% of nodes with nAD between 0.75 and 1.0 μm, and 62% of nodes with nAD > 1.0 μm).

TABLE 2.

Percentage of Nodes Contacted by NG2 cells, Astrocytes, or Both in Different Central Nervous System Regions

Glial cell contact	Spinal cord[1] ($n = 245$)	Optic nerve[2] ($n = 237$)	Corpus callosum[1] ($n = 106$)
NG2 cells (NG2+)	49.8	48.1	33.0
Astrocytes (GLAST+)	98.8	95.4	96.2
Both NG2 cells and astrocytes	49.0	47.3	33.0

[1]Mouse.
[2]Rat.

In the corpus callosum, the nodes of Ranvier were uniformly smaller, with nAD ranging from 0.44 to 1.17 μm, and were contacted by NG2 cell processes less frequently compared with optic nerve and spinal cord (Table 2). There was no difference in the mean nAD of those with and without NG2 cell processes (Fig. 6J; 0.70 ± 0.02 μm, $n = 35$, vs. 0.69 ± 0.02 μm, $n = 71$, respectively, $P > 0.05$). The mean nGW of the nodes with NG2 cell processes was slightly larger than those without (Fig. 6K; 1.53 ± 0.07, $n = 35$, vs. 1.37 ± 0.04 μm, $n = 71$, respectively, $P < 0.05$). A scatterplot of nAD and nGW showed overlapping clusters of nodes with and without NG2 cell processes, with no clear difference in pattern (Fig. 6L). The percentage of nodes containing NG2 cell processes was slightly greater in axons with nAD < 0.75 μm (35%) than those with nAD > 0.75 μm (28%) (Fig. 6M).

NG2+ processes contact nodes with axonal branchpoint

During quantification of nodal contact by glial processes, some nodes of Ranvier in the spinal cord were observed

to be axonal branchpoints. These nodes appeared as areas of AnkG staining flanked by Caspr+ paranodes, but also had AnkG+ projections, which were usually smaller, extending laterally from the node, leading to a third Caspr+ cluster (Fig. 7A–C; see Supplementary movie 3). To investigate whether NG2 cell processes had any preference for contact with these branchpoint (BP) nodes, each node was scored for the presence of a BP. BP nodes accounted for 18.8% of the total number of scored nodes (46/245). Branchpoints were also found to be more frequent in larger axons. The mean nAD of BP nodes was higher than that of nonbranched nodes (Fig. 7D; 0.93 ± 0.02 μm, $n = 199$, vs. 1.19 ± 0.08 μm, $n = 46$, $P < 0.001$). The mean nGW was also significantly larger in branched nodes than nonbranched nodes (Fig. 7E; 1.20 ± 0.06, $n = 46$, vs. 1.09 ± 0.02 μm, $n = 199$, $P < 0.05$). A higher number of BP nodes had an NG2+ process (28/46; 61%) than those that did not (18/46; 39%), which likely reflects the tendency of branchpoints to occur in larger axons. When we excluded BP nodes from the quantification of NG2 cell contacts, NG2 cells were still found to be associated with larger nodes (Fig. 7F; nAD: 1.01 ± 0.04 μm, $n = 94$, vs. 0.86 ± 0.02 μm, $n = 105$ for nonbranched nodes with and without NG2 cell processes, respectively, $P < 0.001$). Similarly, the nGW was greater in nonbranched nodes with NG2 cell processes (Fig. 7G; 1.15 ± 0.03, $n = 94$, vs. 1.05 ± 0.02 μm, $n = 105$, for nonbranched nodes with and without NG2 cell processes, respectively, $P < 0.01$). These values were comparable to those of total nodes (see Fig. 6), suggesting that the association of NG2 cell processes with the node was more closely correlated with the size of the nodal axon rather than the presence of a BP.

Ultrastructural analysis of nodal contact by glial cell processes

To more precisely determine the spatial relationship between nodes of Ranvier and the processes of NG2 cells and astrocytes, pre-embedding immunoelectron microscopy was performed on P30 rat optic nerves

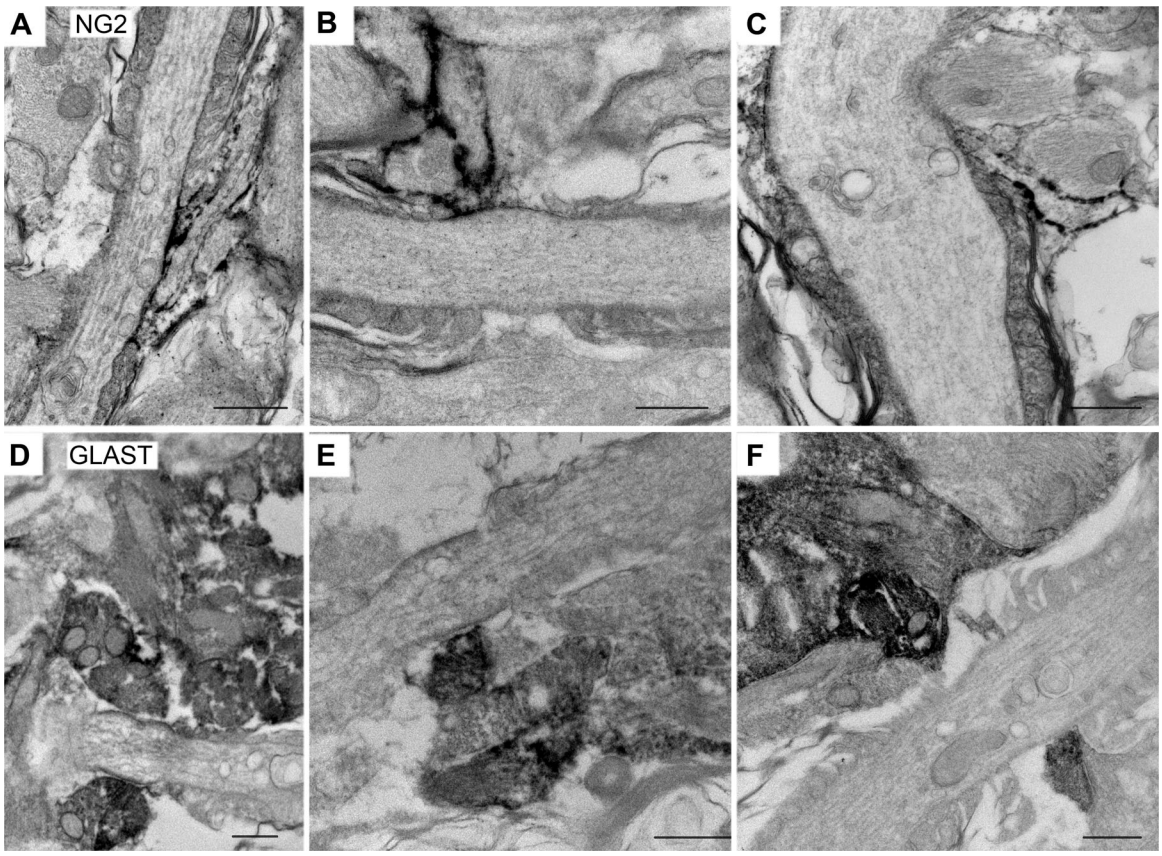

Figure 8. Pre-embedding immunoelectron microscopy of glial cells at the nodes. **A–C:** Immunoperoxidase labeling using rabbit anti-NG2 antibody. **A,B:** P30 rat optic nerve. **C:** P30 mouse optic nerve. Slender immunolabeled NG2+ processes insert into the nodes obliquely and are directly apposed to a portion of the nodal axonal membrane. **D–F:** Immunoperoxidase labeling using guinea pig anti-GLAST antibody. P30 rat optic nerve. GLAST+ processes appear as broad structures that cover the nodal membrane. In most cases, these processes do not seem to directly contact the axolemma. Scale bar = 500 nm in A–F.

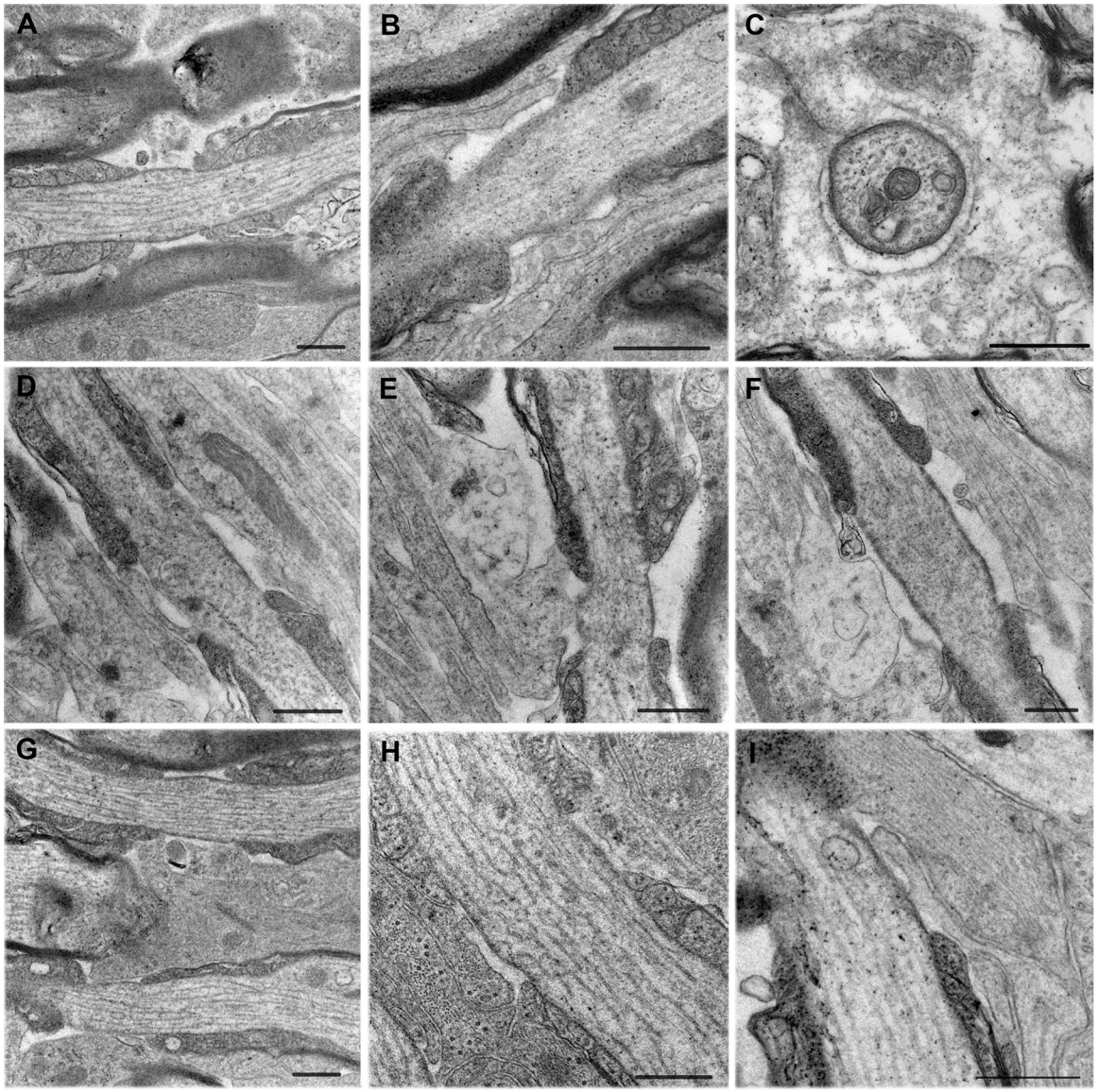

Figure 9. Morphology of glial processes at the nodes. **A:** Longitudinal section of a node that lacks glial cells. There is fuzzy extracellular material around the nodal membrane. **B–F:** Nodes with NG2 cell-like processes. **B:** Slender NG2 cell-like processes. One process contacts both the node and the paranodes. **C:** Cross section through a node that is surrounded by an electron-lucent glial cell process, resembling an NG2 cell process. The process completely surrounds the node and contacts the nodal membrane where the two lips meet. **D:** A thin process contacting the edge of the node and the adjacent paranode. **E:** A wider process also contacting the paranodal surface and the nodal membrane. The light cytoplasm resembles that of NG2 cells rather than that of astrocytes. **F:** A growth cone-like extension of a thin NG2 cell-like process, which surrounds a degenerated tip of the outermost paranodal loop. **G–I:** Nodes with astrocyte-like processes. **G:** A wide astrocyte-like glial process that covers two nodes of parallel axons. **H:** Another example of a node covered by an astrocyte-like wide process. **I:** Longitudinal section through a node that contains a long, thin NG2 cell-like process underneath a thicker astrocyte-like process with bundles of filaments. The astrocytic membrane in G–I does not come into direct contact with the nodal membrane. A,D–I: fixed with 2% paraformaldehyde and 2.5% glutaraldehyde. B,C: fixed with 4% paraformaldehyde and 0.1% glutaraldehyde. A–C,G–I: P30 optic nerve. D–F: P30 corpus callosum. Scale bar = 500 nm in A–I.

using antibodies to NG2 and GLAST. NG2-immunoreactive processes were found to be in contact with the nodal axonal membrane in several nodes (Fig. 8A–C). NG2-labeled processes appeared as long, thin, finger-like projections that extended toward the node obliquely, and in the majority of the cases, they covered only a portion of the nodal axolemma. These slender processes were seen along the outermost paranodal loops of myelin as they contacted the nodes. NG2+ processes had relatively light cytoplasm and did not contain intermediate filaments, but some had various sized vacuoles. Frequently, these vacuolar structures in NG2 cells were

seen immediately beneath the nodal contact surface (Fig. 8B). Often, NG2+ glial processes at the node were seen adjacent to NG2-negative glial processes, which often covered the remaining nodal axonal membrane. These latter glial processes were wider, and some contained bundles of tightly packed filaments that resembled intermediate filaments (Fig. 8C), similar to what had previously been described (Butt et al., 1999), suggesting that they were astrocyte processes. In some cases, NG2-immunoreactive processes were seen on both sides of the axon at the node. There appeared to be a direct membrane apposition between the NG2-immunoreactive process and the nodal axonal membrane.

GLAST-immunoreactive structures at the nodes were much broader than NG2-immunoreactive structures and covered a wider segment of the nodal axonal membrane (Fig. 8D–F). Electron-dense products corresponding to GLAST immunoreactivity were found not only at the plasma membrane but also in the cytoplasm, and thus precluded identification of the fine cytoplasmic structures in the GLAST+ processes. Intermediate filament-like structures were seen in the more proximal wider segments of the labeled processes (Fig. 8D and data not shown).

To further examine the glial insertion at the nodes of Ranvier, P30 optic nerve and corpus callosum were fixed with 2.5% glutaraldehyde and 2% formaldehyde for better preservation of the morphology. We observed nodes with various configurations of glia. A subpopulation of nodes was devoid of glia but was surrounded by fuzzy extracellular matrix material (Fig. 9A). Other nodes were contacted by slender processes with relatively light cytoplasm, resembling NG2-labeled processes (Fig. 9B–F,I). In many cases, the thin, light processes appeared to come into contact with the nodal axonal membrane at discrete points and rarely contacted the entire nodal membrane. Often, these projections made contact with both the nodal membrane and the adjacent paranodal membrane (Fig. 9B,D,E). Such dual nodal and paranodal glial contacts were seen at the nodes in both the optic nerve (Fig. 9B) and corpus callosum (Fig. 9D,E). Figure 9C shows a cross section of a node in the P30 optic nerve that was completely surrounded by a light NG2 cell-like cytoplasmic process, which did not directly contact most of the perimeter of the nodal axon except at one point near the site where the two lips of the glial process came together (Fig. 9C, upper left). We noticed in the corpus callosum that some NG2 cell-like slender processes expanded in a growth cone-like extension near the node (Fig. 9E,F). Figure 9F shows such a growth cone-like expansion that surrounded a short protrusion from the outermost paranodal loop resembling a degenerated loop. The cytoplasm of polydendrocyte-like cells that surrounded the node typically contained various sized clear vacuoles.

Some nodes were covered by electron-dense wide glial processes resembling GLAST+ cells (Fig. 9G–I). In most of the cases where the nodes were covered by such wide astrocyte-like glial processes, there was a narrow space between the glial process and the nodal axonal membrane, and direct contact between the glial process and the axon was rarely seen. Figure 9I shows a thin NG2 cell-like process underneath a broader astrocyte-like process with parallel bundles of filaments. There is some electron-dense material in the extracellular space between the two adjacent glial membranes.

DISCUSSION

Astrocytes surround the majority of the nodes while NG2 cells are more frequently associated with larger nodes

We used quadruple immunofluorescence labeling and confocal microscopy to quantify the extent of NG2 cell and astrocyte apposition at the nodes of Ranvier in three different CNS regions containing different sized axons and provide supportive qualitative observations by super-resolution and electron microscopy. Processes from individual NG2 cells and astrocytes extended to multiple nodes of Ranvier from multiple axons. Nearly all (>95%) nodes in the optic nerve, corpus callosum, and spinal cord contained astrocyte processes. By contrast, NG2 glial insertion occurred in less than half of nodes in all three regions, and, intriguingly, NG2 cell processes were more frequently associated with nodes having larger nodal axon diameter and larger nodal gap width. In the corpus callosum where the axons were the smallest, NG2 cell processes were present at only one-third of the nodes, with no preference for axon size. In the slightly larger axons of the optic nerve, the frequency of nodal NG2 cell contact increased with nodal axon diameter. This tendency was more prominent among the large axons in the ventral funiculus of the spinal cord, where 65% of the nodes with nAD > 1.25 μm were contacted by NG2 cell processes.

Ultrastructural analysis also revealed the heterogeneity of the nodes with respect to glial ensheathment. Some nodes had extensive glial apposition, whereas other nodes showed no glial coverage in the plane of the ultrathin section. There were differences in the manner in which NG2 cells and astrocytes inserted their processes at the node, as schematized in Figure 10. Astrocyte processes were often broader and surrounded a greater portion of the nodal axonal membrane. By contrast, NG2 cell processes were more slender, and appeared to form contacts at discrete

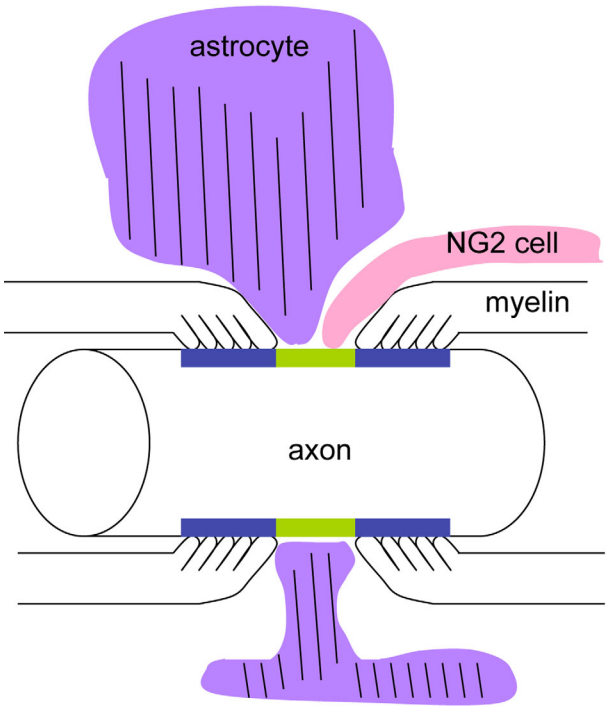

Figure 10. A scheme depicting a node of Ranvier contacted by an astrocyte (purple) and an NG2 cell (pink). The nodal axolemma is indicated in green and the paranodal membrane in blue. An astrocyte process that contains glial filaments (parallel lines) broadly surrounds the node, whereas an NG2 cell process is more slender and finger-like, coming into contact both at the node and on the myelin paranodal surface.

points on the axonal membrane. In many cases, they contacted both the nodal axonal membrane and the outer surface of the oligodendrocyte paranodal membrane in a discontinuous manner (Figs. 8B,D,E, 9). At some nodes, NG2 cells formed a ring around the node/paranode junction (Fig. 4A–C).

STED super-resolution microscopy is an emerging technique that uses depletion laser beams to overcome the resolution limit of light microscopy posed by diffraction of light (Hell and Wichmann, 1994). This technique, which can be used on multilabeled tissue sections, revealed NG2 cell processes as thin projections that made punctate and/or looping contacts at the nodal axonal membrane, while astrocytes appeared as broader sheet-like processes with extensions to the node (Fig. 5). There was extensive intertwining of the processes of astrocytes and NG2 cells, as previously reported outside the nodal region (Nishiyama et al., 2002; Hamilton et al., 2010).

Hildebrand (1971) described the glia at the node as perinodal astrocyte processes and noted the presence of glial filaments in some of them that were oriented perpendicularly to the axons, as seen here (Fig. 8C). Using HNK-1 antibody, ffrench-Constant et al. (1986) saw small HNK1+ processes at the node that were distinct from HNK-1–negative large astrocytic processes. More than a decade later, Butt et al. (1999) showed NG2 immunoreactivity on a nodal glial process and suggested that NG2 cells could correspond to the previously identified perinodal glia, which left unanswered the question of the frequency of the occurrence of the two glial cell types at the node. Our quantification revealing that the vast majority of the nodes are surrounded by astrocytes, while 33–50% of them have NG2 cell insertions, provides a resolution to this debate and suggests distinct roles for astrocytes and NG2 cells at the node.

The role of nodal glia

Nodal astrocytes could play a role in clearing extracellular potassium released by neuronal activity (Kimelberg, 2010), and the broad processes of astrocytes that surround the nodes could facilitate this role. Perinodal astrocytes but not NG2 cells abundantly express the glial glutamate transporter GLAST, and astrocytes in the white matter have been shown to take up glutamate (Arranz et al., 2008; Domercq et al., 2005). Furthermore, vesicularly released glutamate from axons in the corpus callosum activates ionotropic glutamate receptors on NG2 cells (Ziskin et al., 2007; Kukley et al., 2007). However, the exact site of release of glutamate is not known. We did not observe any accumulation of clear vesicles underneath the nodal axolemma apposed by NG2 cells as previously reported for “axoglial junctions” in other CNS regions (Peters et al., 1991).

The role of NG2 glia in the physiology of the nodes of Ranvier remains unknown. One obvious role is to differentiate into oligodendrocytes and produce internodes. Recent genetic fate mapping studies indicate that production of new oligodendrocytes and myelin is a dynamic process that continues in the adult CNS and is influenced by neural activity (Young et al., 2013; Hill and Nishiyama, 2014; Hill et al., 2014; Gibson et al., 2014). Furthermore, generation of new myelin is critical for learning new motor skills (McKenzie et al., 2014). An NG2 cell that loops around the node while also making a contact on the paranodal membrane is in a strategic position to detect changes in the state of myelin and transform into a myelinating cell when needed. Figure 9F shows a growth cone–like extension of a polydendrocyte-like cell apposed to an extension of the outermost paranodal loop that appears degenerated (Fig. 9F). NG2 cells synthesize matrix metalloproteinases (Seo et al., 2013) and could be involved in tissue

maintenance and remodeling at the node/paranodal junction.

NG2 cells and astrocytes secrete extracellular matrix (ECM), which could affect the function of the node. On most nodes, the axonal membrane was only partially contacted by the glial processes, leaving a significant portion of it exposed to the ECM. The lectican family of chondroitin sulfate proteoglycans, which includes the nodal proteins brevican and versican, represents a major class of ECMs. These proteoglycans form a large polymer and regulate cellular functions by providing a reservoir for growth factors and modulating axonal growth during development and after injury (Fawcett, 2015; Maeda, 2015). Brevican is highly expressed by both astrocytes and NG2 cells (Zhang et al., 2014) and is involved in nodal assembly through its association with the axonal cell surface adhesion molecule neurofascin-186 (Sherman et al., 2005; Susuki et al., 2013). Versican-V2 recruits another ECM molecule, tenascin-R, which in turn recruits phosphacan, a cleavage product of receptor protein tyrosine phosphatase-beta (RPTP-β) (Dours-Zimmermann et al., 2009), and NG2 cells are the major source of versican-V2, tenascin-R, and RPTP-β; Zhang et al., 2014). It is possible that NG2 cells contribute to maintaining the structural integrity of the nodal axon, particularly the larger axons that they were found to associate with.

The role of NG2 cells in axonal growth has been controversial (Nishiyama et al., 2009). It has been suggested that perinodal NG2 cells could inhibit collateral sprouting from the node, although it is not known whether versican-V2, which is produced by NG2 cells (Chang et al., 2010) and was erroneously reported as oligodendrocyte-myelin glycoprotein (Omg) in an earlier study (Huang et al., 2005), has an axon-inhibitory function. The role for NG2 cells observed at nodal branchpoints remains unclear.

NG2 can be cleaved from the membrane, particularly around the node of Ranvier in peripheral axons (Martin et al., 2001) and in the injured CNS (Stallcup and Huang, 2008). However, our pre-embedding immunolabeling showed NG2 to be exclusively localized to cell surface and did not reveal any ECM labeling. Intriguingly, injection of NG2 but not lecticans into the thoracic white matter of the adult spinal cord caused a dose- and time-dependent reduction in the amplitude of evoked potentials recorded from lumbar spinal motor neurons after stimulation of cervical cord (Hunanyan et al., 2010). Furthermore, in the injured spinal cord, where NG2 accumulates extracellularly, injection of anti-NG2 antibodies prevented conduction block and promoted behavioral recovery (Petrosyan et al., 2013). While we do not know the mechanism of how extracellular NG2 regulates the action potentials, nor do we know the relevance of these observations to the function of NG2 cells in the normal CNS axon where NG2 remains membrane-bound, these observations suggest a role for nodal glia and ECM in regulating functional plasticity in the white matter.

Why are some nodes contacted by NG2 glial cell processes while others are not? Myelin around larger diameter axons that are more frequently contacted by NG2 cells may be turning over more rapidly than myelin ensheathing smaller axons. It is also possible that the glial ensheathment of the nodal membrane is dependent on or reflects the activity of the axon.

In summary, this study provides the first quantitative simultaneous assessment of the frequency of astrocyte and NG2 cell processes at the central nodes of Ranvier. The use of specific antibodies to NG2 cells and astrocytes allowed unequivocal simultaneous visualization of the two non-overlapping glial cell types at the node. Our observation that $>$95% of the nodes are surrounded by astrocyte processes while 33–50% are also contacted by NG2 cell processes clarifies ambiguities of earlier studies that had used the term “glia” or “astrocytes” collectively to refer to both astrocytes and NG2 cells and provides the anatomical foundation for future investigations on the role of astrocytes and NG2 cells in white matter plasticity.

ACKNOWLEDGMENTS

We thank Youfen Sun for maintaining the animal colony and her assistance with tissue sectioning. We thank Dr. Matt Rasband (Baylor College of Medicine) for the rabbit anti-Caspr antibody and Dr. William Stallcup (Sanford Burnham Institute) for the rabbit and guinea pig anti-NG2 antibodies. We thank Dr. Christine Hanko (Leica Microsystems) for expert assistance with STED imaging and Dr. Chris O’Connell (Confocal Microscope Facility, University of Connecticut) for his assistance with confocal and STED microscopy.

CONFLICT OF INTEREST

The authors declare no conflicts of interest.

ROLE OF AUTHORS

All authors had full access to all the data in the study and take full responsibility for the integrity of the data and the accuracy of the data analysis. The study was initially conceived and designed by DRS and AN. PJ, who subsequently joined the laboratory, designed additional studies. DRS performed immunolabeling and electron microscopy. PJ performed immunofluorescence

labeling, 3D analysis, and all the quantifications. AN coordinated all the experiments. All authors wrote the original manuscript. PJ and AN revised the manuscript, and all authors contributed to the figures and the final manuscript content.

REFERENCES

Amor V, Feinberg K, Eshed-Eisenbach Y, Vainshtein A, Frechter S, Grumet M, Rosenbluth J, Peles E. 2014. Long-term maintenance of Na+ channels at nodes of Ranvier depends on glial contact mediated by gliomedin and NrCAM. J Neurosci 34:5089–5098.

Arranz AM, Hussein A, Alix JJ, Perez-Cerda F, Allcock N, Matute C, Fern R. 2008. Functional glutamate transport in rodent optic nerve axons and glia. Glia 56:1353–1367.

Bergles DE, Jabs R, Steinhauser C. 2010. Neuron-glia synapses in the brain. Brain Res Rev 63:130–137.

Bhat RV, Axt KJ, Fosnaugh JS, Smith KJ, Johnson KA, Hill DE, Kinzler KW, Baraban JM. 1996. Expression of the APC tumor suppressor protein in oligodendroglia. Glia 17: 169–174.

Brandao KE, Dell'Acqua ML, Levinson SR. 2012. A-kinase anchoring protein 150 expression in a specific subset of TRPV1- and CaV 1.2-positive nociceptive rat dorsal root ganglion neurons. J Comp Neurol 520:81–99.

Brill MH, Waxman SG, Moore JW, Joyner RW. 1977. Conduction velocity and spike configuration in myelinated fibres: computed dependence on internode distance. J Neurol Neurosurg Psychiatry 40:769–774.

Butt AM, Duncan A, Hornby MF, Kirvell SL, Hunter A, Levine JM, Berry M. 1999. Cells expressing the NG2 antigen contact nodes of Ranvier in adult CNS white matter. Glia 26:84–91.

Chang KJ, Susuki K, Dours-Zimmermann MT, Zimmermann DR, Rasband MN. 2010. Oligodendrocyte myelin glycoprotein does not influence node of ranvier structure or assembly. J Neurosci 30:14476–14481.

Chung EK, Chen LW, Chan YS, Yung KK. 2008. Downregulation of glial glutamate transporters after dopamine denervation in the striatum of 6-hydroxydopamine-lesioned rats. J Comp Neurol 511:421–437.

Dagley LF, White CA, Liao Y, Shi W, Smyth GK, Orian JM, Emili A, Purcell AW. 2014. Quantitative proteomic profiling reveals novel region-specific markers in the adult mouse brain. Proteomics 14:241–261.

Damiani D, Novelli E, Mazzoni F, Strettoi E. 2012. Undersized dendritic arborizations in retinal ganglion cells of the rd1 mutant mouse: a paradigm of early onset photoreceptor degeneration. J Comp Neurol 520:1406–1423.

Domercq M, Etxebarria E, Perez-Samartin A, Matute C. 2005. Excitotoxic oligodendrocyte death and axonal damage induced by glutamate transporter inhibition. Glia 52:36–46.

Dours-Zimmermann MT, Maurer K, Rauch U, Stoffel W, Fassler R, Zimmermann DR. 2009. Versican V2 assembles the extracellular matrix surrounding the nodes of ranvier in the CNS. J Neurosci 29:7731–7742.

Douyard J, Shen L, Huganir RL, Rubio ME. 2007. Differential neuronal and glial expression of GluR1 AMPA receptor subunit and the scaffolding proteins SAP97 and 4.1N during rat cerebellar development. J Comp Neurol 502: 141–156.

Fawcett JW. 2015. The extracellular matrix in plasticity and regeneration after CNS injury and neurodegenerative disease. Prog Brain Res 218:213–226.

ffrench-Constant C, Miller RH, Kruse J, Schachner M, Raff MC. 1986. Molecular specialization of astrocyte processes at nodes of Ranvier in rat optic nerve. J Cell Biol 102:844–852.

Gasser A, Ho TS, Cheng X, Chang KJ, Waxman SG, Rasband MN, Dib-Hajj SD. 2012. An ankyrinG-binding motif is necessary and sufficient for targeting Nav1.6 sodium channels to axon initial segments and nodes of Ranvier. J Neurosci 32:7232–7243.

Gibson EM, Purger D, Mount CW, Goldstein AK, Lin GL, Wood LS, Inema I, Miller SE, Bieri G, Zuchero JB, Barres BA, Woo PJ, Vogel H, Monje M. 2014. Neuronal activity promotes oligodendrogenesis and adaptive myelination in the mammalian brain. Science 344:1252304.

Hamilton N, Vayro S, Wigley R, Butt AM. 2010. Axons and astrocytes release ATP and glutamate to evoke calcium signals in NG2-glia. Glia 58:66–79.

Hell, SW Wichmann J. 1994. Breaking the diffraction resolution limit by stimulated emission: stimulated-emission-depletion fluorescence microscopy. Optics Lett 19:780–782

Hildebrand C. 1971. Ultrastructural and light-microscopic studies of the nodal region in large myelinated fibres of the adult feline spinal cord white matter. Acta Physiol Scand Suppl 364:43–79.

Hill RA, Nishiyama A. 2014. NG2 cells (polydendrocytes): listeners to the neural network with diverse properties. Glia 62:1195–1210.

Hill RA, Patel KD, Goncalves CM, Grutzendler J, Nishiyama A. 2014. Modulation of oligodendrocyte generation during a critical temporal window after NG2 cell division. Nat Neurosci 17:1518–1527.

Huang JK, Phillips GR, Roth AD, Pedraza L, Shan W, Belkaid W, Mi S, Fex-Svenningsen A, Florens L, Yates JR 3rd, Colman DR. 2005. Glial membranes at the node of Ranvier prevent neurite outgrowth. Science 310:1813–1817.

Hunanyan AS, Garcia-Alias G, Alessi V, Levine JM, Fawcett JW, Mendell LM, Arvanian VL. 2010. Role of chondroitin sulfate proteoglycans in axonal conduction in mammalian spinal cord. J Neurosci 30:7761–7769.

Kimelberg HK. 2010. Functions of mature mammalian astrocytes: a current view. Neuroscientist 16:79–106.

King AN, Manning CF, Trimmer JS. 2014. A unique ion channel clustering domain on the axon initial segment of mammalian neurons. J Comp Neurol 522:2594–2608.

King CH, Lancaster E, Salomon D, Peles E, Scherer SS. 2014. Kv7.2 regulates the function of peripheral sensory neurons. J Comp Neurol 522:3262–3280.

Komitova M, Zhu X, Serwanski DR, Nishiyama A. 2009. NG2 cells are distinct from neurogenic cells in the subventricular zone. J Comp Neurol 512:702–715.

Komitova M, Serwanski DR, Nishiyama A. 2011. NG2 cells are not a major source of reactive astrocytes in neocortical stab wound. Glia 59:800–809.

Kukley M, Capetillo-Zarate E, Dietrich D. 2007. Vesicular glutamate release from axons in white matter. Nat Neurosci 10:311–320.

Lasiene J, Matsui A, Sawa Y, Wong F, Horner PJ. 2009. Age-related myelin dynamics revealed by increased oligodendrogenesis and short internodes. Aging Cell 8:201–213.

Maeda N. 2015. Proteoglycans and neuronal migration in the cerebral cortex during development and disease. Front Neurosci 9:98.

Martin S, Levine AK, Chen ZJ, Ughrin Y, Levine JM. 2001. Deposition of the NG2 proteoglycan at nodes of Ranvier in the peripheral nervous system. J Neurosci 21:8119–8128.

McKenzie IA, Ohayon D, Li H, de Faria JP, Emery B, Tohyama K, Richardson WD. 2014. Motor skill learning requires active central myelination. Science 346:318–322.

McLean IW, Nakane PK. 1974. Periodate-lysine-paraformaldehyde fixative. A new fixation for immunoelectron microscopy. J Histochem Cytochem 22:1077–1083.

Nishiyama A, Watanabe M, Yang Z, Bu J. 2002. Identity, distribution, and development of NG2+ glial cells. J Neurocytol 31:437–455.

Nishiyama A, Komitova M, Suzuki R, Zhu X. 2009. Polydendrocytes (NG2 cells): multifunctional cells with lineage plasticity. Nat Rev Neurosci 10:9–22.

Normand EA, Rasband MN. 2015. Subcellular patterning: axonal domains with specialized structure and function. Dev Cell 32:459–468.

Peles E, Nativ M, Lustig M, Grumet M, Schilling J, Martinez R, Plowman GD, Schlessinger J 1997. Identification of a novel contactin-associated transmembrane receptor with multiple domains implicated in protein-protein interactions. EMBO J 16:978–988.

Peters A. 2004. A fourth type of neuroglial cell in the adult central nervous system. J Neurocytol 33:345–357.

Peters A, Palay SL, deF Webster H. 1991. The fine structure of the nervous system. New York: Oxford.

Petrosyan HA, Hunanyan AS, Alessi V, Schnell L, Levine J, Arvanian VL. 2013. Neutralization of inhibitory molecule NG2 improves synaptic transmission, retrograde transport, and locomotor function after spinal cord injury in adult rats. J Neurosci 33:4032–4043.

Rasband MN, Peles E, Trimmer JS, Levinson SR, Lux SE, Shrager P. 1999. Dependence of nodal sodium channel clustering on paranodal axoglial contact in the developing CNS. J Neurosci 19:7516–7528.

Rasband MN, Kagawa T, Park EW, Ikenaka K, Trimmer JS. 2003. Dysregulation of axonal sodium channel isoforms after adult-onset chronic demyelination. J Neurosci Res 73:465–470.

Schafer DP, Bansal R, Hedstrom KL, Pfeiffer SE, Rasband MN. 2004. Does paranode formation and maintenance require partitioning of neurofascin 155 into lipid rafts? J Neurosci 24:3176–3185.

Seidl AH, Rubel EW, Harris DM. 2010. Mechanisms for adjusting interaural time differences to achieve binaural coincidence detection. J Neurosci 30:70–80.

Seo JH, Miyamoto N, Hayakawa K, Pham LD, Maki T, Ayata C, Kim KW, Lo EH, Arai K. 2013. Oligodendrocyte precursors induce early blood-brain barrier opening after white matter injury. J Clin Invest 123:782–786.

Sherman DL, Tait S, Melrose S, Johnson R, Zonta B, Court FA, Macklin WB, Meek S, Smith AJ, Cottrell DF, Brophy PJ. 2005. Neurofascins are required to establish axonal domains for saltatory conduction. Neuron 48:737–742.

Shibata T, Yamada K, Watanabe M, Ikenaka K, Wada K, Tanaka K, Inoue Y. 1997. Glutamate transporter GLAST is expressed in the radial glia-astrocyte lineage of developing mouse spinal cord. J Neurosci 17:9212–9219.

Stallcup WB, Huang FJ. 2008. A role for the NG2 proteoglycan in glioma progression. Cell Adh Migr 2:192–201.

Susuki K, Chang KJ, Zollinger DR, Liu Y, Ogawa Y, Eshed-Eisenbach Y, Dours-Zimmermann MT, Oses-Prieto JA, Burlingame AL, Seidenbecher CI, Zimmermann DR, Oohashi T, Peles E, Rasband MN. 2013. Three mechanisms assemble central nervous system nodes of Ranvier. Neuron 78:469–482.

Tillet E, Gential B, Garrone R, Stallcup WB 2002. NG2 proteoglycan mediates beta1 integrin-independent cell adhesion and spreading on collagen VI. J Cell Biochem 86: 726–736.

Tomassy GS, Berger DR, Chen HH, Kasthuri N, Hayworth KJ, Vercelli A, Seung HS, Lichtman JW, Arlotta P. 2014. Distinct profiles of myelin distribution along single axons of pyramidal neurons in the neocortex. Science 344:319–324.

Waxman SG, Black JA. 1984. Freeze-fracture ultrastructure of the perinodal astrocyte and associated glial junctions. Brain Res 308:77–87.

Waxman SG, Swadlow HA. 1976. Ultrastructure of visual callosal axons in the rabbit. Exp Neurol 53:115–127.

Yamanaka H, Kobayashi K, Okubo M, Fukuoka T, Noguchi K. 2011. Increase of close homolog of cell adhesion molecule L1 in primary afferent by nerve injury and the contribution to neuropathic pain. J Comp Neurol 519:1597–1615.

Young KM, Psachoulia K, Tripathi RB, Dunn SJ, Cossell L, Attwell D, Tohyama K, Richardson WD. 2013. Oligodendrocyte dynamics in the healthy adult CNS: evidence for myelin remodeling. Neuron 77:873–885.

Zhang Y, Chen K, Sloan SA, Bennett ML, Scholze AR, O'Keeffe S, Phatnani HP, Guarnieri P, Caneda C, Ruderisch N, Deng S, Liddelow SA, Zhang C, Daneman R, Maniatis T, Barres BA, Wu JQ. 2014. An RNA-sequencing transcriptome and splicing database of glia, neurons, and vascular cells of the cerebral cortex. J Neurosci 34:11929–11947.

Zhu X, Bergles DE, Nishiyama A. 2008. NG2 cells generate both oligodendrocytes and gray matter astrocytes. Development 135:145–157.

Ziskin JL, Nishiyama A, Rubio M, Fukaya M, Bergles DE. 2007. Vesicular release of glutamate from unmyelinated axons in white matter. Nat Neurosci 10:321–330.